

Supporting Information

High Energy Density Aqueous Zinc-Benzoquinone Battery Enabled by Carbon Cloth with Multiple Anchoring Effects

Zhiqiang Luo, Silin Zheng, Shuo Zhao, Xin Jiao, Zongshuai Gong, Fengshi Cai, Yueqin Duan, Fujun Li, and Zhihao Yuan**

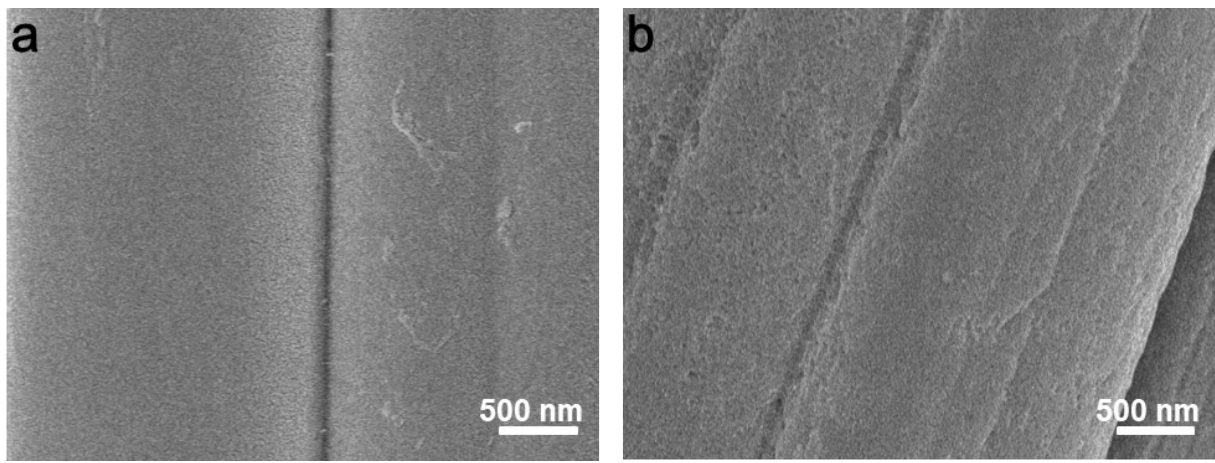


Fig. S1. SEM images of a) untreated CC and b) plasma treatment CC (NCC).

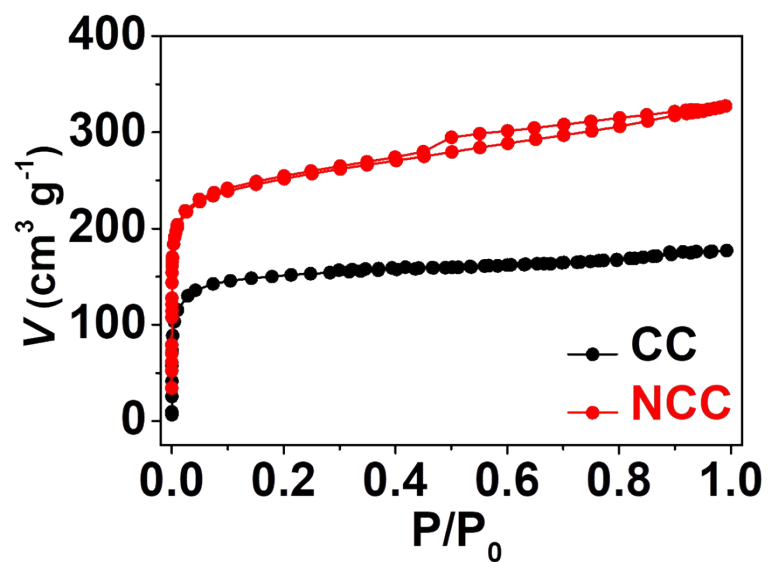


Fig. S2. N_2 adsorption-desorption isotherms for CC and NCC.

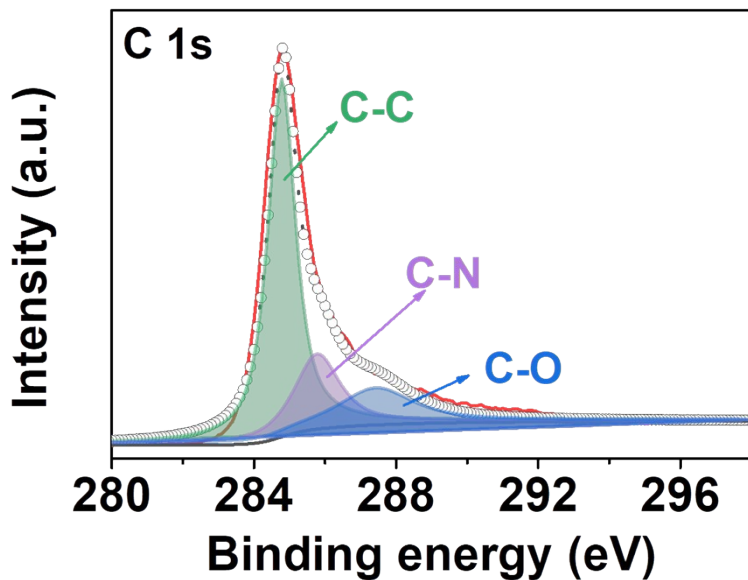


Fig. S3. High resolution XPS C1s spectrum of NCC.

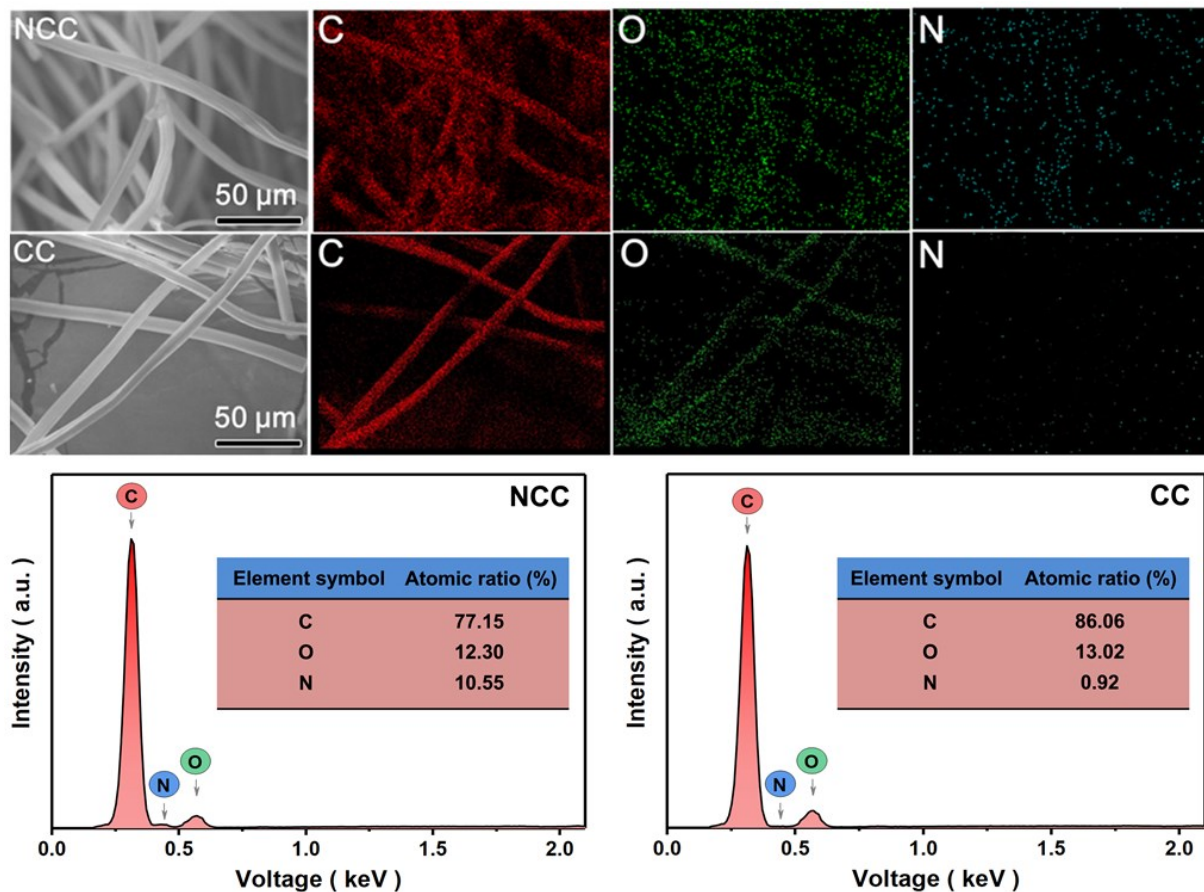


Fig. S4. EDS mapping images of NCC and CC host. The EDS elemental mapping images further reveal the homogeneous distribution of C, O, and N, indicating the successfully incorporated N element into CC.

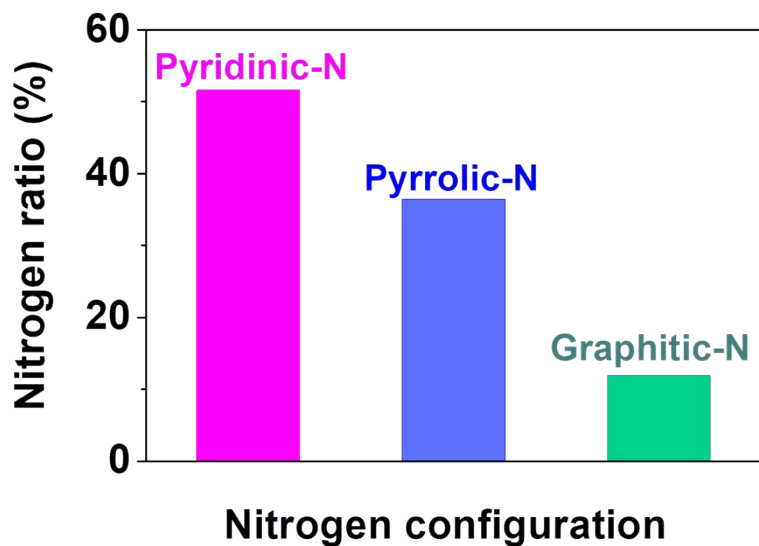


Fig. S5. The content of the pyridinic-, pyrrolic-, and graphitic-N atom.

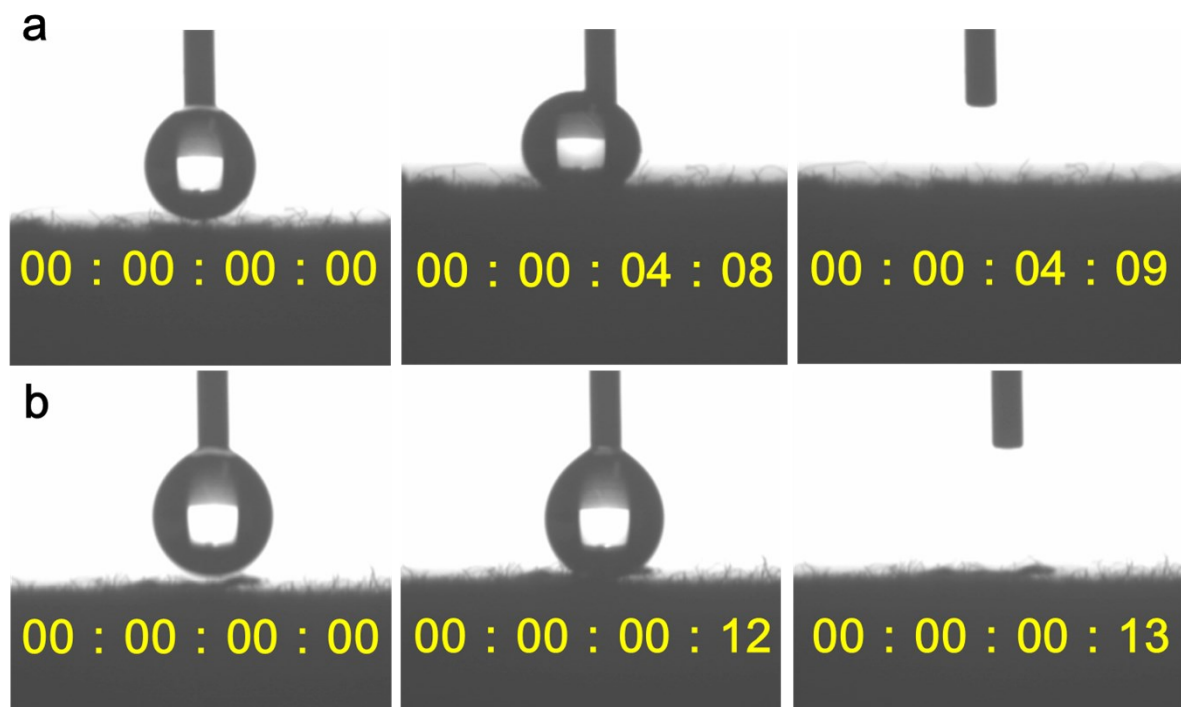


Fig. S6. The wettability test of (a) CC and (b) NCC.

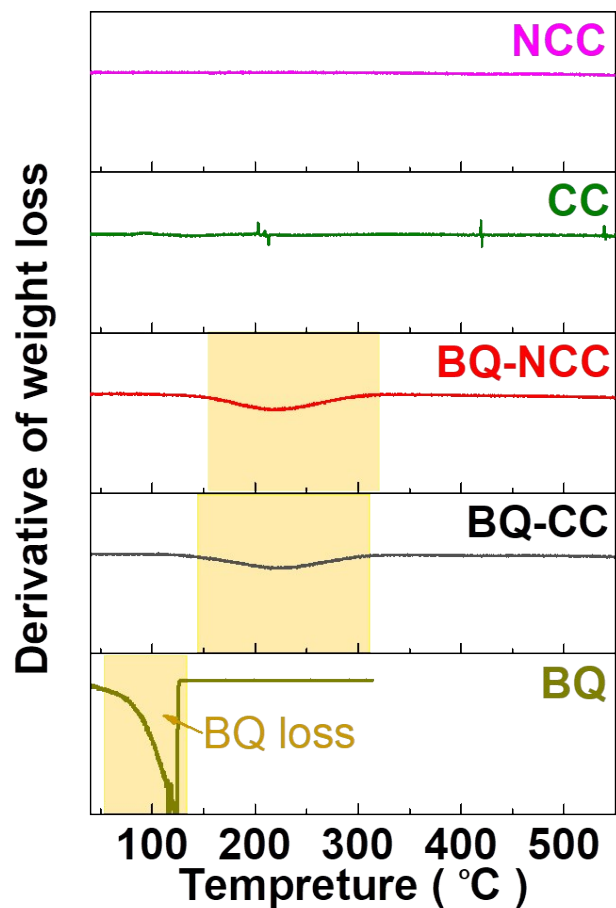


Fig. S7. DTA curves of BQ, CC, NCC, BQ-CC and BQ-NCC.

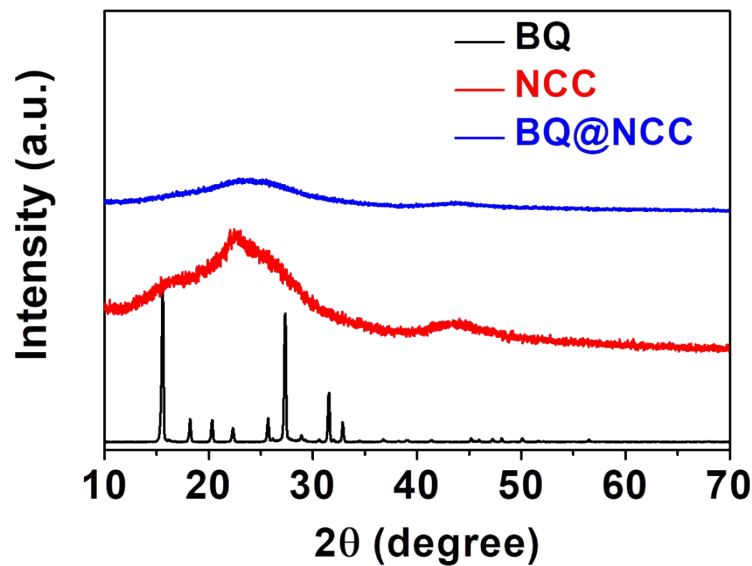


Fig. S8. XRD patterns of pure BQ, NCC, and BQ ($\sim 4.5 \text{ mg/cm}^2$) on NCC.

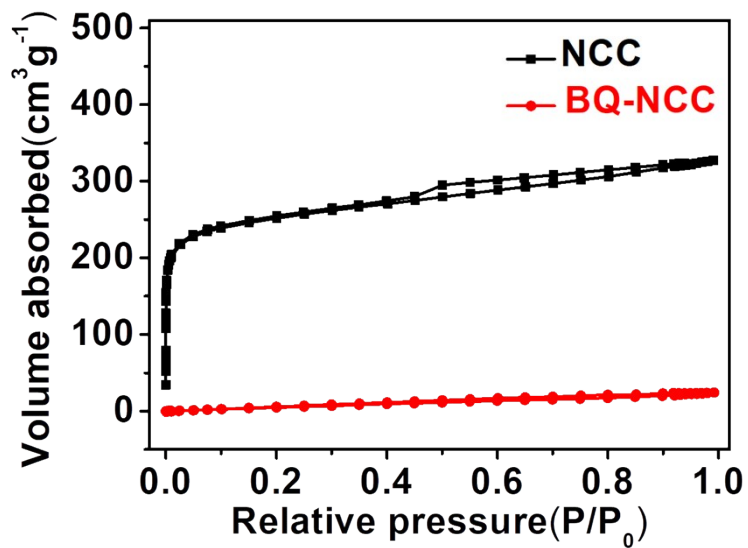


Fig. S9. N_2 adsorption-desorption isotherm of NCC and BQ-NCC.

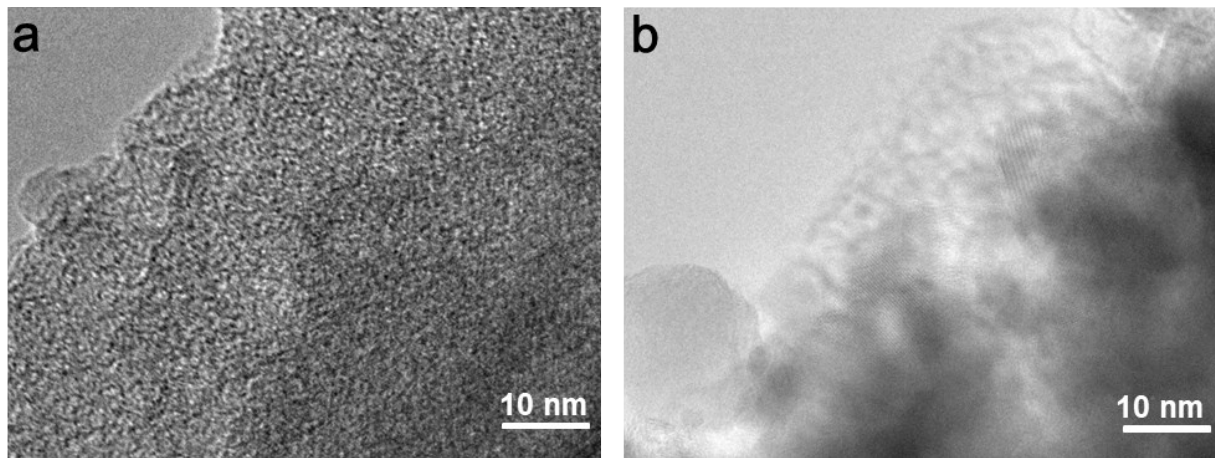


Fig. S10. TEM images of pristine NCC (a) and BQ-NCC (b).

From TEM images of NCC, we can observe the pores in these carbon materials. After adsorbing BQ, the pores are filled with BQ.

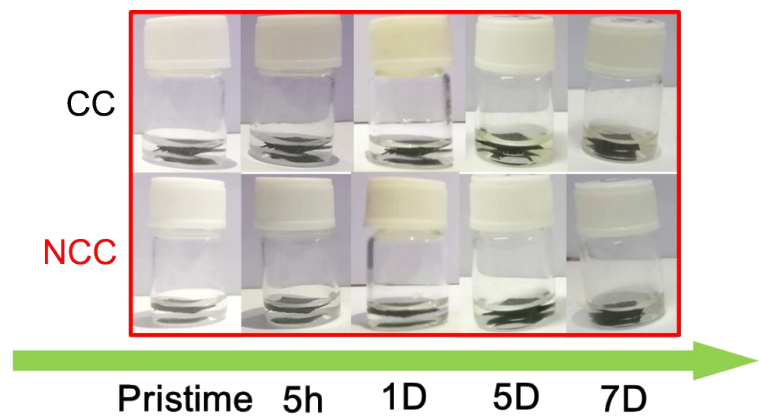


Fig. S11. Photographs of the BQ-CC and BQ-NCC electrodes immersed in the electrolyte (2 ml; 3 M ZnSO₄) for different time intervals.

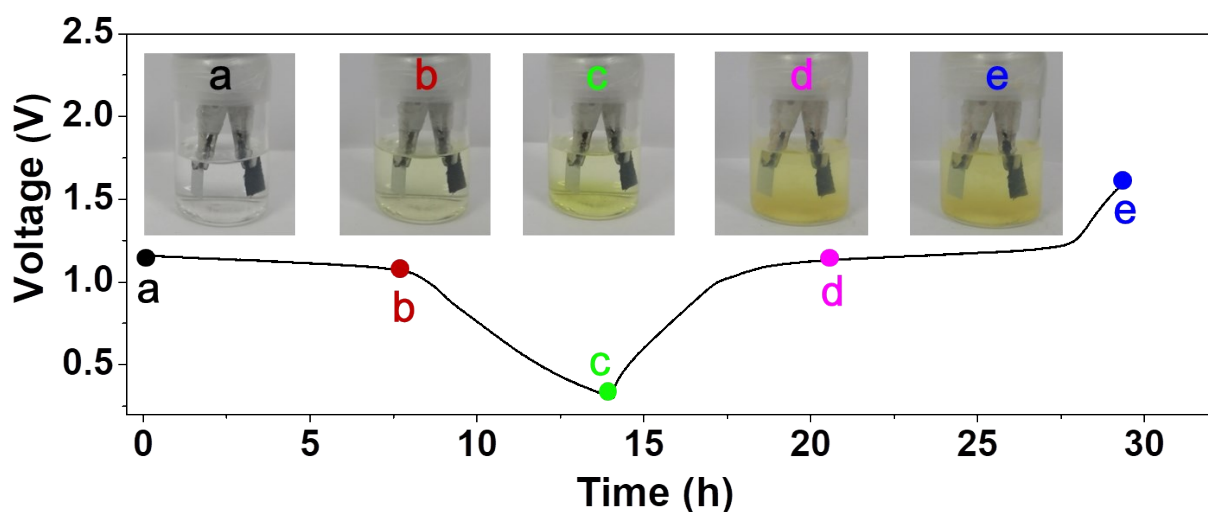


Fig. S12. Visual images of the discharge and charge process of a Zn//BQ-CC batteries at different states.

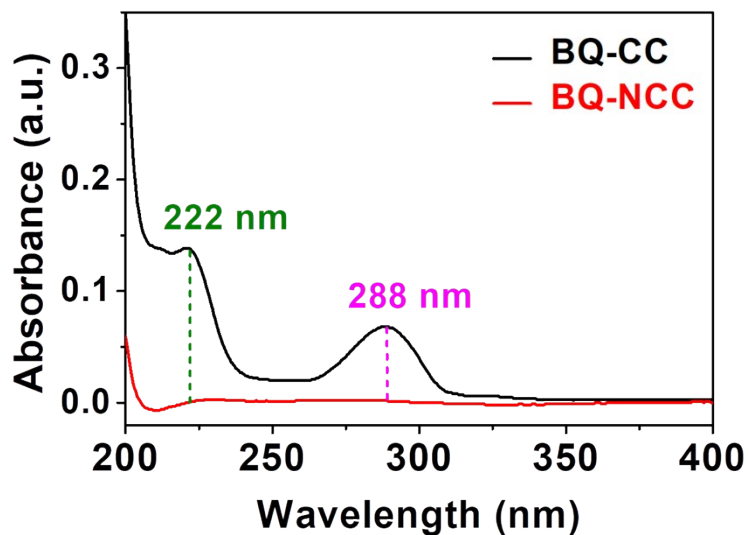


Fig. S13. The UV-Vis spectra of electrolytes after discharge of BQ-CC and BQ-NCC electrodes.

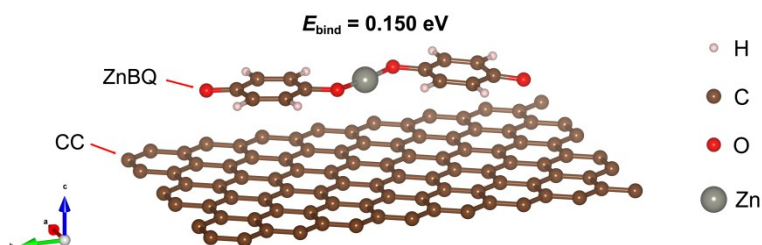


Fig. S14. The calculated structure of ZnBQ adsorption on graphene.

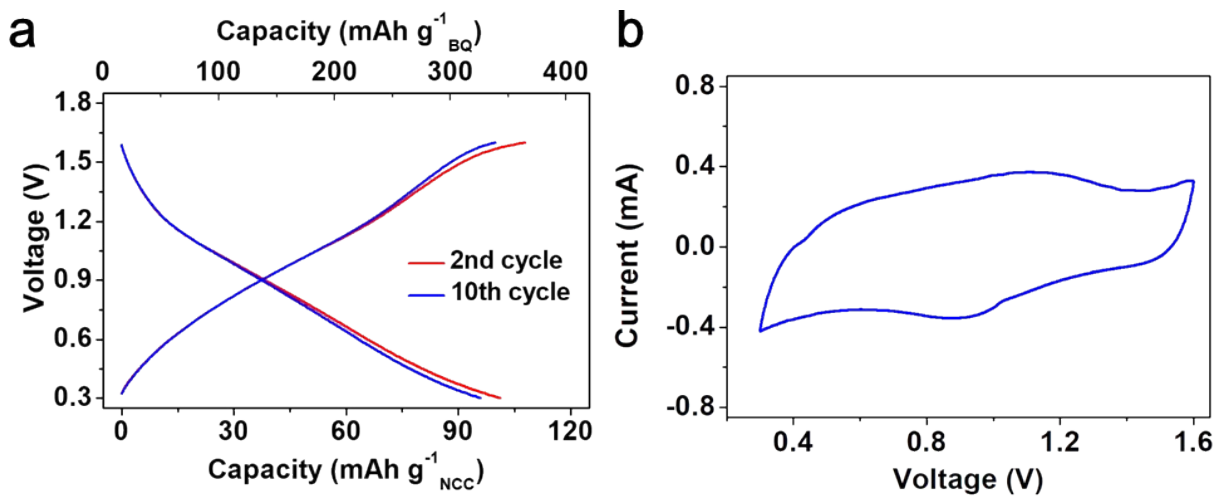


Fig. S15. (a) Typical discharge and charge curves of blank NCC at the second and tenth cycles at the same current density of 0.1 A g^{-1} . (b) Cyclic voltammetry curve of blank NCC at a rate of 0.1 mV s^{-1} . The capacity of blank NCC is 101 mAh g^{-1} based on $\sim 15 \text{ mg}$ of NCC in an electrode pellet, corresponding to 337.8 mAh g^{-1} of BQ with a mass loading of $\sim 4.5 \text{ mg}$.

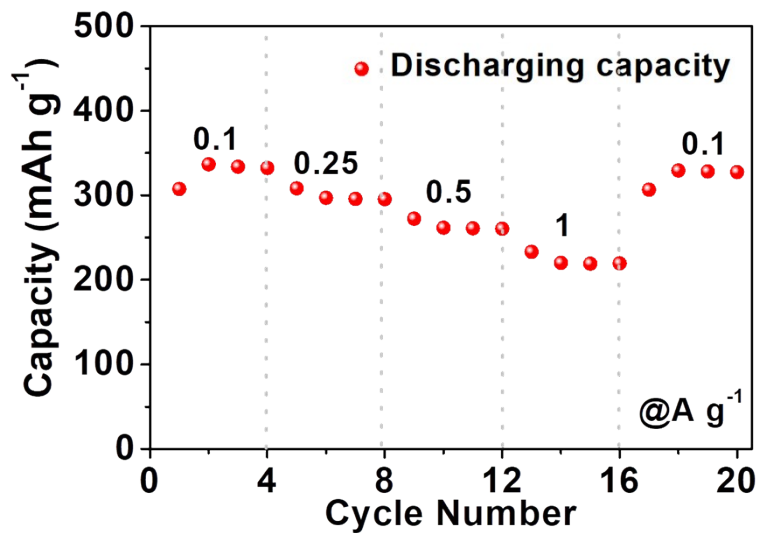


Fig. S16. Capacitance behaviour of NCC at different current density of $0.1, 0.25, 0.5$, to 1 A g^{-1} . The NCC delivers the discharge capacities of $337.8, 297.2, 261.6$, and 216.9 mAh g^{-1} (by mass of BQ $\sim 4.5 \text{ mg cm}^{-2}$), respectively.

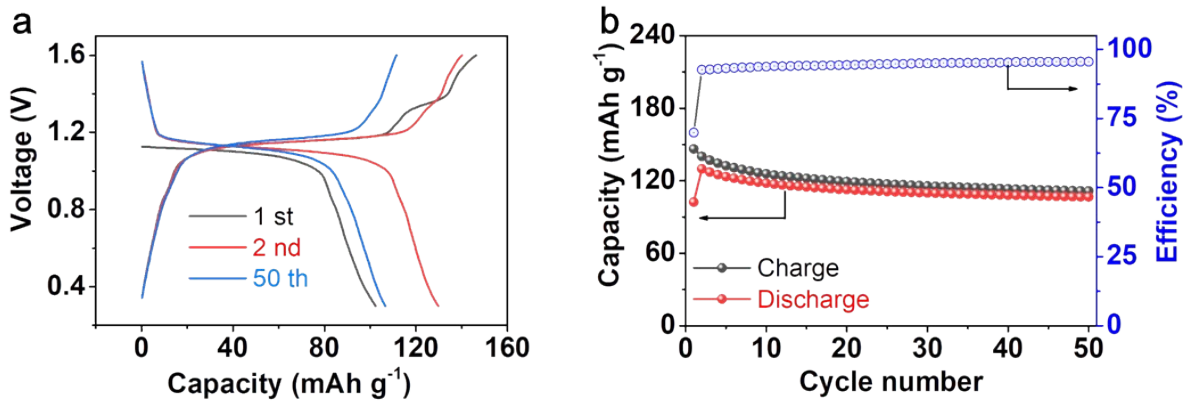


Fig. S17. (a) Typical discharge and charge curves (a) and corresponding cycling performance (b) of BQ cathode with stainless steel foil current collector at 0.1 A g^{-1} .

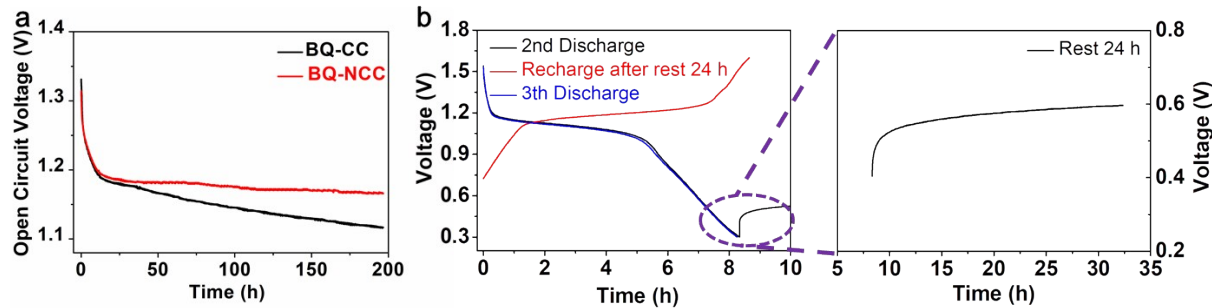


Fig. S18. (a) The open-circuit voltage of BQ-NCC and BQ-CC fresh cells during original storage. (b) Self-discharge behavior of BQ-NCC tested at a current density of 0.2 A g^{-1} , when secondly discharged to 0.3V after rest for 24 hours, and then charged to 1.6 V, and thirdly discharged to 0.3V.

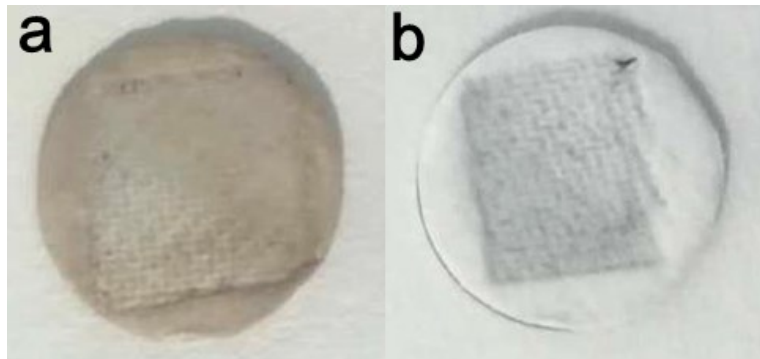


Fig. S19. The optical photograph of cycled separator with a) BQ-CC and b) BQ-NCC electrode.

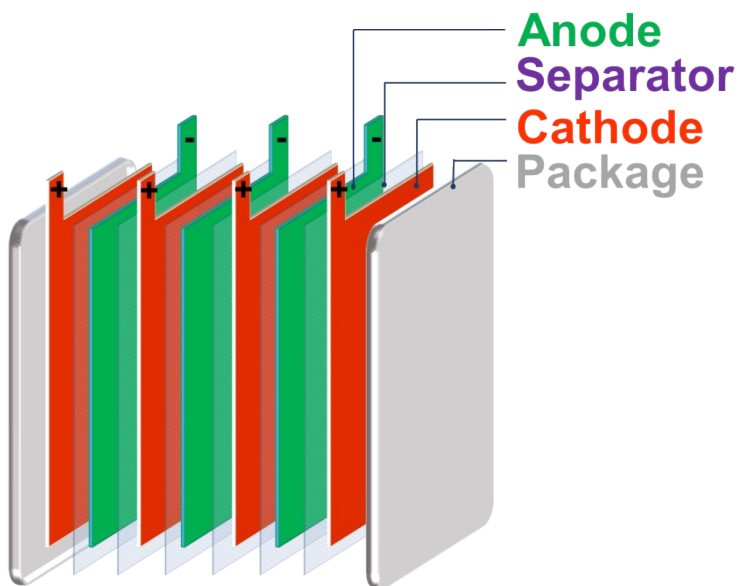


Fig. S20. The schematic diagram shows the packaging technology of a pouch Zn//BQ-NCC cell.

Calculation about energy density of the aqueous Zn//BQ-NCC battery:

The energy density of the aqueous Zn//BQ-NCC battery is detailed calculated as follows (based on the practical utilization of BQ-NCC and Zn foil):

BQ-NCC cathode is 1.26 g (inclusion 0.3 g BQ and 0.96 g NCC), in which the theoretical capacity is 248.04 mA h ($0.3 \text{ g} \times 826.8 \text{ mA h g}^{-1}$). In practical test, the pouch-type cell displayed a capacity of 228.9 mA h after discharging to the voltage of 0.3 V. The DOD (depth of discharge) is 92.3% ($228.9 \div 248.04 \times 100\%$). The theoretical consumption zinc anode is 0.28 g ($228.9 \text{ mA h} \div 820 \text{ mA h g}^{-1}$). The practical mass of zinc foil is 0.592 g (thickness:

0.02 mm), thus the practical utilization of zinc anode is up to 47.4% ($0.28 \text{ g} \div 0.59 \text{ g}$) in pouch-type cell. Calculations about the energy density of pouch cell is 163.5 Wh kg^{-1} $\{(0.2289 \text{ A h} \times 1.1 \text{ V}) \div [(1.26 + 0.28) \times 10^{-3} \text{ kg}]\}$ (corresponding to 136.1 Wh kg^{-1} by the total mass of BQ, Zn foil and NCC host).

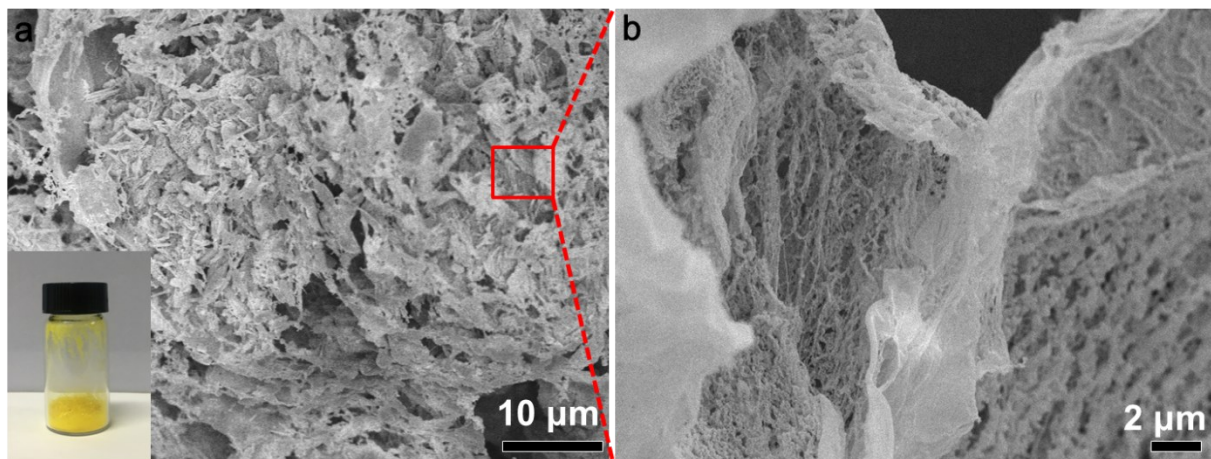


Fig. S21. The pure BQ powder in a vial, exhibit the yellow based color, the SEM image of a) pure BQ and b) the enlarged image.

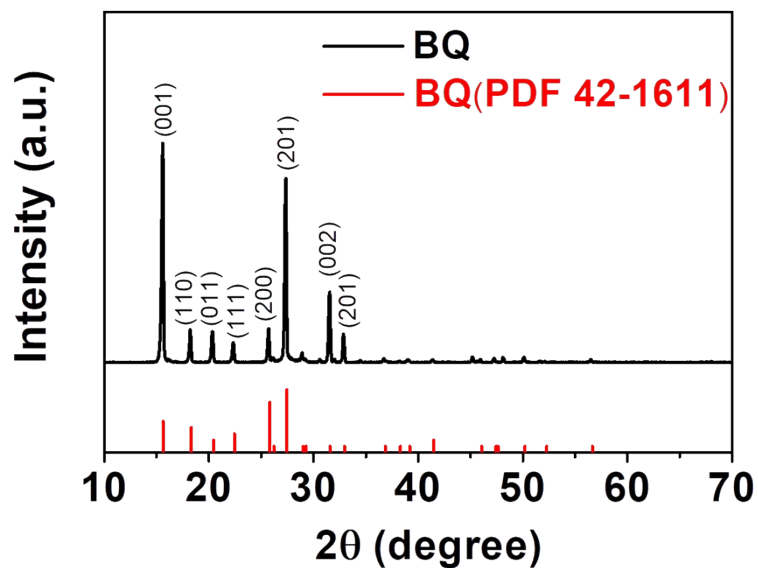


Fig. S22. XRD patterns of BQ. The crystal structure of BQ is indicated by XRD pattern and corresponds to the JCPDS card (42-1611).

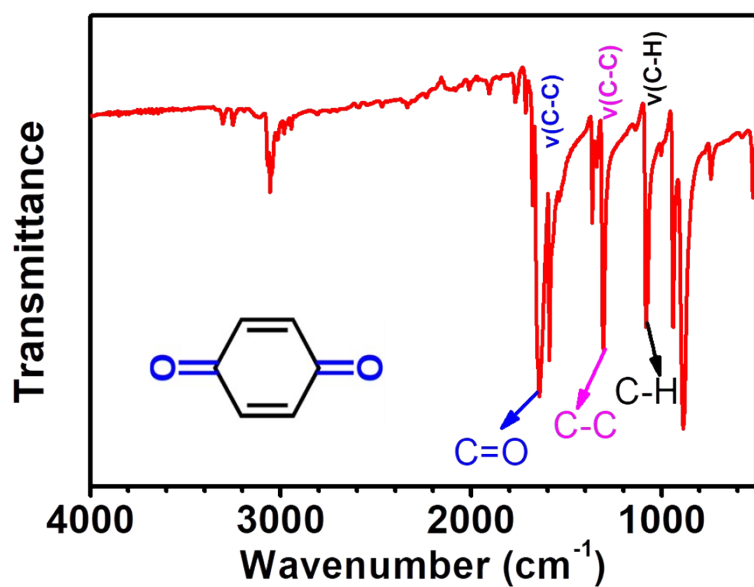


Fig. S23. Fourier transform infrared spectroscopy (FTIR) spectra of purified BQ sample.

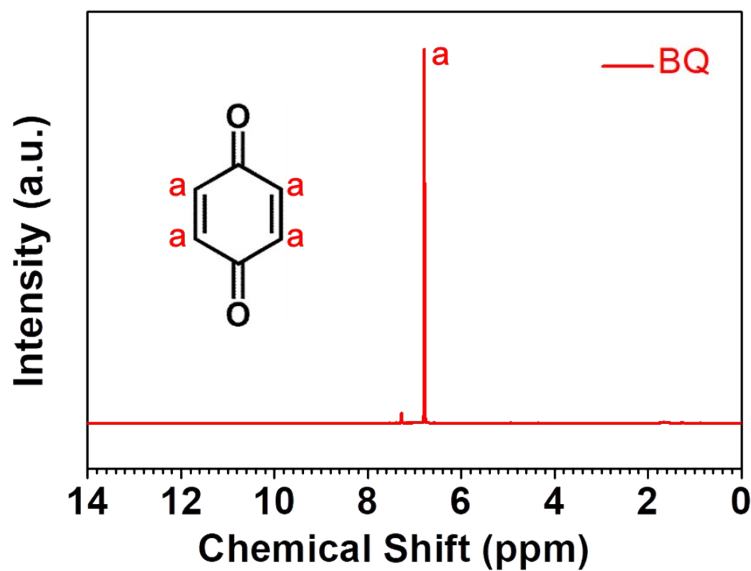


Fig. S24. ^1H spectrum of BQ (400 MHz, TFA-d, 298 K).



Scheme S1. Schematic illustrating the fabrication of BQ-NCC composite electrodes via a simply “solution-adsorption” process.

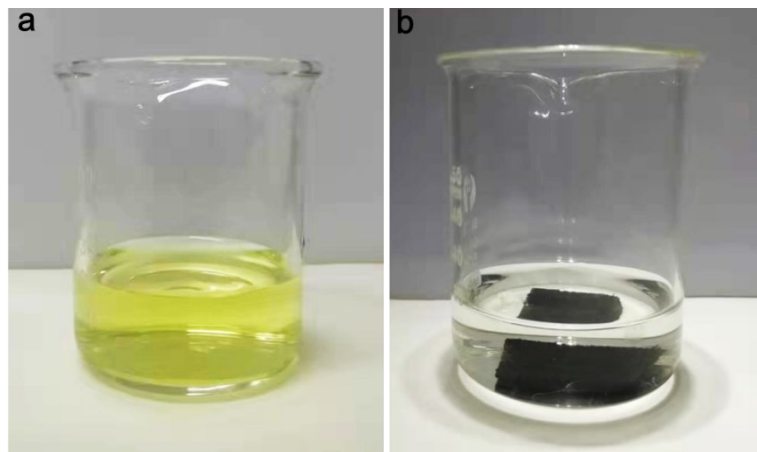


Fig. S25. Digital photograph of preparing BQ-NCC cathode, showing that BQ was adsorbed on NCC (20 ml distilled water /20 mg BQ, 4 cm² NCC).

Table S1. Comparison of energy density between this work and typically reported inorganic and organic compound as cathode for AZBs.

Refs.	Cathode material	Testing voltage range (V), operating voltage (V)	Discharge capacity (mAh g ⁻¹), at current density (mA g ⁻¹)	Electrolyte (aqueous)	Energy Density (Wh kg ⁻¹) ^{a)}
S1	KCuFe(CN) ₆	- , 0.6	56, ~20	1 M ZnSO ₄	33.6
S2	Zn ₃ [Fe(CN) ₆] ₂	0.8-2.0, 1.57	65.4, 60	1 M ZnSO ₄	102.7
S3	α -MnO ₂ @graphene	1.0-1.85, 1.25	362.2, 300	2 M ZnSO ₄ 0.2 M MnSO ₄	452.7
S4	MnO ₂	1.0-1.8, 1.37	366.6, 74	2 M ZnCl ₂ , 0.4 M MnSO ₄	502.2
S5	Zn _{0.25} V ₂ O ₅ nH ₂ O	0.5-1.4, 0.9	300, 50	1 M ZnSO ₄	270
S6	V ₂ O ₅ ·nH ₂ O	0.2-1.6, 0.91	381, 60	3 M Zn(CF ₃ SO ₃) ₂	346.7
S7	V ₂ O ₅	0.2-1.6, 0.72	470, 200	3 M Zn(CF ₃ SO ₃) ₂	338.4
S8	P-chloranil	0.8-1.4, 1.1	205, 43.4	1 M Zn(CF ₃ SO ₃) ₂	225.5
S9	C4Q	0.8-1.3, 1.0	335, 20	3 M Zn(CF ₃ SO ₃) ₂	335
S10	PQ- Δ	0.25-1.6, 0.78	210, 150	3 M Zn(CF ₃ SO ₃) ₂	163.8
S11	PTO	0.4-1.5, 0.9	336, 40	2 M ZnSO ₄	302.4
This work	BQ-NCC	0.3-1.6 V, 1.1 V	489, 100	3 M ZnSO ₄	537.9

Note: a)The values are calculated based on the discharge capacity of cathode.

Table S2. Price of battery subassembly.

	Price (\$ kg ⁻¹)	Reference
Zn	2.27	<i>Energy Storage Mater.</i> 2020 , 28, 247–254.
BQ	2.2	https://marketpublishers.com/r/PBF6D0E3848EN.html
ZnSO ₄	2.8	https://marketpublishers.com/report/non_ferrous_metallurgy/zinc/global-zinc-sulphate-market-outlook-2016-2021.html

References

- [S1] R. Trocoli, F. La Mantia, *Chem. Sus. Chem.* 2015, *8*, 481–485.
- [S2] L. Zhang, L. Chen, X. Zhou, Z. Liu, *Adv. Energy Mater.* 2015, *5*, 1400930.
- [S3] B. Wu, G. Zhang, M. Yan, T. Xiong, P. He, L. He, X. Xu, L. Mai, *Small* 2018, *14*, 1703850.
- [S4] Y. Zeng, X. Zhang, Y. Meng, M. Yu, J. Yi, Y. Wu, X. Lu, Y. Tong, *Adv. Mater.* 2017, *29*, 1700274.
- [S5] D. Kundu, B. D. Adams, V. Duffort, S. H. Vajargah, L. F. Nazar, *Nat. Energy* 2016, *1*, 16119.
- [S6] M. Yan, P. He, Y. Chen, S. Wang, Q. Wei, K. Zhao, X. Xu, Q. An, Y. Shuang, Y. Shao, K. T. Mueller, L. Mai, J. Liu, J. Yang, *Adv. Mater.* 2018, *30*, 1703725.
- [S7] J. Zhou, L. Shan, Z. Wu, X. Guo, G. Fang, S. Liang, *Chem. Commun.* 2018, *54*, 4457–4460.
- [S8] D. Kundu, P. Oberholzer, C. Glaros, A. Bouzid, E. Tervoort, A. Pasquarello, M. Niederberger, *Chem. Mater.* 2018, *30*, 3874–3881.
- [S9] Q. Zhao, W. Huang, Z. Luo, L. Liu, Y. Lu, Y. Li, L. Li, J. Hu, H. Ma, J. Chen, *Sci. Adv.* 2018, *4*, eaao1761.
- [S10] K. W. Nam, H. Kim, Y. Beldjoudi, T. Kwon, D. J. Kim, J. F. Stoddart, *J. Am. Chem. Soc.* 2020, *142*, 2541–2548.
- [S11] Z. Guo, Y. Ma, X. Dong, J. Huang, Y. Wang, Y. Xia, *Angew. Chem. Int. Ed.* 2018, *57*, 11737–1174.